CSCE 2021 Annual Conference
Inspired by Nature – Inspiré par la Nature

26-29 May 2021

THE APPLICABILITY OF THE TWO-FLUID MODEL TO SIMULATE SOIL INTERNAL FLUIDIZATION DUE TO PIPE LEAKAGE

Ibrahim, A[1], and Meguid, M[2]
[1] Graduate student, Department of Civil Engineering and Applied Mechanics, McGill University, ahmed.ibrahim5@mail.mcgill.ca
[2] Professor, Department of Civil Engineering and Applied Mechanics, McGill University, mohamed.meguid@mcgill.ca

Abstract: Internal fluidization in soils due to pipe leakage can compromise the integrity and strength of surrounding soils causing softening and deformation that could pose threats to nearby structures. Analyzing the coupled dynamics of soil-water interactions at the microscale level is needed to adequately understand the mechanism and extent of fluidization. Despite the existence of models that can accurately perform this coupling, it remains computationally expensive and often impractical to perform on a large scale that represents actual situations. In this study, we explore the potential of using the Two-Fluid Model (TFM) to simulate internal fluidization as a computationally feasible and scalable model. Numerical simulations of a pressurized water jet into a submerged sand bed are carried out and the results are compared with experimental data and other numerical results. The analysis presented in this study shows a good agreement between the proposed TFM approach and both experimental and numerical simulation in terms of excess pore water pressure values and the extent of the fluidized zone. The model limitations arising from the continuum representation are then highlighted. The model's performance indicates that it is a viable tool for the preliminary assessment of soil-water coupling problems involving leaking watermains and similar problems in ground engineering.

1 INTRODUCTION

Internal soil fluidization and erosion can happen in the vicinity of leaking buried pipes due to local pressure increase and rapid water flow within the surrounding soil. When fluidized, the soil loses some or all of its shear strength (i.e., liquefied) due to the increase in pore water pressure. This can compromise the soil integrity, strength and ultimately leads to volume loss and the formation of sinkholes (Ali and Choi 2019, Karoui et al. 2018). Characterizing and predicting internal fluidization of soils can be particularly challenging considering the complex underlying physics that govern fluidization (Cui et al. 2014). These physics involve the interaction mechanisms, momentum transfer and force balance between soil particles and water, or other fluids (Zhu et al. 2007). This type of analysis has been widely adopted in fluidized beds, where

fluidization is induced by gas or liquid injection through an opening (Tsuji, Kawaguchi, and Tanaka 1993, Ostermeier et al. 2019, Deen et al. 2007). In ground engineering and earth structure, with less controlled environment than this of fluidized beds, the analysis becomes more complex as the properties of soils such as cohesion and particle size variability come to play a major role (Suzuki et al. 2007, Zou, Chen, and Zhang 2020). Furthermore, if a hydraulic transient is to occur in a compromised leaking pipe, more complex interactions are to happen as the pressure wave travels back and forth across the system.

Analyzing internal fluidization requires access to information related to the micromechanics of the system and resolving the particle-fluid interaction. Several attempts have been made to investigate these interactions experimentally (Alsaydalani 2010, van Zyl et al. 2013), numerically (Cui et al. 2014) and using simplified analytical models (Montella et al. 2016, Vardoulakis, Stavropoulou, and Papanastasiou 1996). Given the limited flexibility of experimental and analytical solutions in obtaining microscale information and dealing with a wide range of initial and boundary conditions, numerical analysis is mostly adopted. The two most common approaches are pure continuum analysis and coupled discrete-continuum analysis. In pure continuum analysis, the solid and fluid phases are treated as a single continuum with collective properties that account for the presence of both phases (i.e., a mixture). Alternatively, the two phases are interpreted as inter-penetrating continua each representing a single phase such as the case of the Two-Fluid Model (TFM) (Anderson and Jackson 1967, Kuipers et al. 1992, Gidaspow 1994). On the other hand, in coupled discrete-continuum analysis the solid phase receives a discrete Lagrangian treatment while the fluid phase is considered as a continuum. Examples for this type of analysis involve the coupled Discrete Element Model-Computational Fluid Dynamics (DEM-CFD) (Tsuji, Tanaka, and Ishida 1992) and Discrete Element Model-Lattice Boltzmann Model (DEM-LBM) (Cook, Noble, and Williams 2004).

Although utilizing discrete methods such as DEM-CFD allows for a relatively more accurate representation of the soil-water coupling compared to continuum-based approaches, it comes at a high computational cost (Ibrahim and Meguid 2020). On the contrary, coupled continuum modelling such as the TFM is much more computationally feasible with code execution time of approximately 7% of this of CFD-DEM (Hirche, Birkholz, and Hinrichsen 2019). Thus, it allows for analyzing larger and more realistic systems and producing results than can be incorporated into conventional analysis needed for design and risk assessment. The application of the TFM, however, has so far been limited to a few cases in simulating sediment transport and riverbed morphology (Chauchat et al. 2017, Cheng, Hsu, and Calantoni 2017). The model's performance is yet to be tested in dealing with earth structures where soils are densely packed and quasi-static flow conditions are most likely to be dominant.

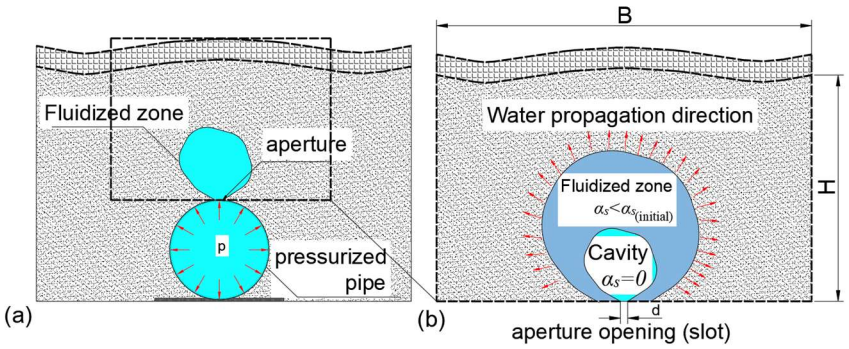

Figure 1: Schematic diagrams for the onset of fluidization: (a) Illustration of the formation of internal fluidization in the vicinity of a leaking pipe; (b) A conceptual representation of the fluidization parameters around the aperture.

In this study, we aim to explore the potential of the TFM to simulate internal fluidization around leaking pressurised pipe (Figure 1(a)). The test case consists of a buried pressurised pipe with an aperture, through which, a water jet is released into the overlying sand layer leading to internal fluidization that can lead to the formation of a water-filled cavity (Figure 1(b)). We investigate the ability of the model to capture the extent of the fluidized zone and the associated changes in pore water pressure. Emphasis is placed on identifying the drawback and limitations of the TFM approach in analyzing soil fluidization caused by water leakage in subsurface structures.

2 NUMERICAL ANALYSIS

The TFM used in this study was developed following the local volume-averaging technique proposed by Anderson and Jackson (1967). In this model, the particulate phase is considered as a fluid-like continuum with equivalent pressure and shear stress flow parameters that reflect the granular behaviour of solids. Thus, the core of this model is the constitutive relationships (closures) used to obtain these parameters. Significant developments to these closures have been made since they were early presented by Anderson and Jackson (1967) such as the Kinetic Theory of Granular Flow (KTGF) (Gidaspow 1994, Jenkins and Savage 1983, Lun et al. 1984, van der Hoef et al. 2006) and granular rheology (Revil-Baudard and Chauchat 2013, Cheng, Hsu, and Calantoni 2017). The governing equations for the TFM consist of the locally averaged continuity and momentum equations. The conservation of mass for both phases can be written as (Chauchat et al. 2017):

$$\frac{\partial \rho^f \alpha^f}{\partial t} + \frac{\partial \rho^f \alpha^f u_i^f}{\partial x_i} = 0, \tag{1}$$

$$\frac{\partial \rho^s \alpha^s}{\partial t} + \frac{\partial \rho^s \alpha^s u_i^s}{\partial x_i} = 0. \tag{2}$$

where α^f and α^s are the volume fractions of both fluid and solid phases such that $\alpha^f + \alpha^s = 1$, ρ^f and ρ^s are the mass densities and u_i^f and u_i^s are (i^{th}) components the cell-averaged velocities of fluid and solid phases, respectively (i.e., u_x, u_y or u_z in cartesian coordinates). Similarly, the conservation of momentum is written as:

$$\frac{\partial \rho^f \alpha^f u_i^f}{\partial t} + \frac{\partial \rho^f \alpha^f u_i^f u_j^f}{\partial x_i} = -\alpha^f \frac{\partial p}{\partial x_i} + \alpha^f f_i + \alpha^f \rho^f g_i + \frac{\partial \tau_{ij}^f}{\partial x_j} - \alpha^f \alpha^s K\left(u_i^f - u_i^s\right), \tag{3}$$

$$\frac{\partial \rho^s \alpha^s u_i^s}{\partial t} + \frac{\partial \rho^s \alpha^s u_i^s u_j^s}{\partial x_i} = -\alpha^s \frac{\partial p}{\partial x_i} + \alpha^s f_i + \alpha^s \rho^s g_i - \frac{\partial \bar{p}^s}{\partial x_i} + \frac{\partial \tau_{ij}^s}{\partial x_j} + \alpha^f \alpha^s K\left(u_i^f - u_i^s\right). \tag{4}$$

where p is the fluid pressure, f_i and g_i are the external and driving body forces and the gravitational acceleration, τ_{ij}^f is the shear stress tensor of the fluid phase, τ_{ij}^s and $\bar{p}^s$ are the shear and normal stresses of the solid phase, and K is the drag parameter. The last term of the right-hand side of Equations (3) and (4) represents the drag force between the two phases associate with particle-fluid interaction, hence it appears in opposite signs such that Newton's third law of motion is not violated.

The solid granular phase is essentially discrete, such that macro-scale or domain-averaged pressure and shear forces are determined from the collective forces acting on individual particles. However, the continuum representation of the solid phase in Equations (2) and (4) does not allow for direct discrete treatment of the solid particles. Thus, closures are needed to obtain the equivalent granular pressure and shear stresses as cell-averaged values. In this study, the closures obtained from the Kinetic Theory of Granular flow are adopted (Gidaspow 1994, Ding and Gidaspow 1990). The solid granular pressure, $\bar{p}^s$, consists of two components: permanent contact pressure, p^{ff}, and shear induced pressure p^s (Johnson and Jackson 1987):

$$\bar{p}^s = p^{ff} + p^s \tag{5}$$

where the permanent contact component is expressed as:

$$p^{ff} = \begin{cases} 0 & \alpha^s < \alpha_{\min}^{Fric}, \\ Fr\frac{\left(\alpha^s - \alpha_{\min}^{Fric}\right)^{\eta_0}}{(\alpha_{max} - \alpha^s)^{\eta_1}} & \alpha^s \geq \alpha_{\min}^{Fric} \end{cases} \tag{6}$$

where Fr, η_0 and $\eta_1$are empirical parameters that take the values of 0.05, 3 and 5, respectively (Cheng, Hsu, and Calantoni 2017). $\alpha_{\min}^{Fric}$ is the minimum solid fraction considered for interparticle friction to develop, for spherical particles, $\alpha_{\min}^{Fric} \approx 0.57$. and α_{max} is the maximum value of solid volume fraction. Special attention should be given to the terms in Equation (6) to avoid diving by zero when $\alpha_{max} = \alpha^s$. This is especially critical in the case when initial settlement of solid particles is required (i.e., static condition). If the initial solid fraction value was set close to α_{max}, numerical instabilities will develop and most likely will lead to a numerical singularity. In order to avoid this, a reasonable margin should be given between the initial and maximum packing values such that the desired initial condition can be achieved without causing instabilities.

The shear-induced granular pressure depends mainly on the granular temperature of the system, Θ, the radial distribution function, g_{s0}, and the coefficient of restitution, e, where the values of the shear-induced pressure is given by Ding and Gidaspow (1990). The simulation was carried out using sedFoam solver (Cheng, Hsu, and Calantoni 2017) on OpenFOAM CFD platform. The solver is an isothermal incompressible version of the twoPhaseEulerFoam solver in OpenFOAM, which is a two-phase solver for solid-fluid flows. The closures of the KTGF presented herein are incorporated in the solver for pressure and shear stress estimation in the solid phase.

3 MODEL VALIDATION

To test the validity of the TFM to simulate internal fluidization, we set up a numerical model to reproduce the experimental study reported by Alsaydalani (2010) and the numerical study performed using Discrete Element Model-Lattice Boltzmann Model (DEM-LBM) by Cui et al. (2014). Both studies tackle the problem

of internal fluidization in a submerged sand bed subjected to a local controlled water injection that resembles water leakage from a buried pipe. One of the important reasons we chose to validate the model using the two aforementioned studies is to test the model's scalability. As opposed to CFD-DEM model, the continuum nature of the TFM allows for local mesh refinement around narrow openings and complex geometry. This can be much more computationally efficient as the need to use a large number of particles no longer exists. It is worth noting that the mean particle size for the numerical study of Cui et al. (2014) is approximately 4.5 times larger than that used in the experiment to reduce the computational cost. Consequently, the slot opening size is increased to 10 times larger. Thus, the scalability of the model presented in this study is put the test to see if this limitation can be overcome by refining the computational mesh around the injection slot.

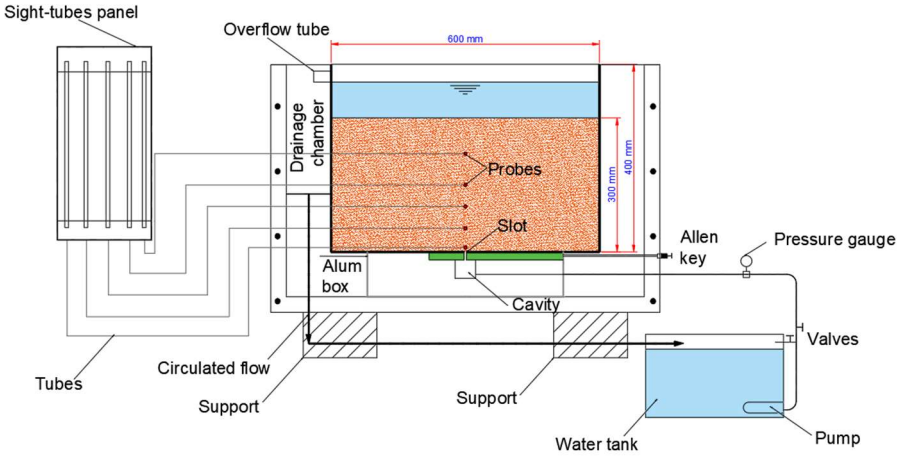

Figure 2. A schematic of the experimental setup [adapted from Alsaydalani (2010).

The experimental setup consists of a box filled with submerged silica sand (sand bed), while water is injected at controlled flow rates through a rectangular slot at the bottom of the box (Figure 2). Probes to measure the excess pore water pressure are placed along the centreline of the box and connected to sight-tubes to measure the development of excess pore water pressure throughout the experiment. Snapshots of the deformation of the sand bed are taken throughout the experiment to monitor the surface heave and the extent of the fluidized zone. For the numerical simulation considered in this study, the height of sand inside the box is set to 0.3 m with two cases for average particle sizes of 1 mm and 4.5 mm corresponding to slot openings of 0.33 mm and 3 mm, respectively. A summary of the simulation parameters for both cases is shown in Table 1.

Table 1: Summary of simulation parameters used by Cui et al. (2014) and Alsaydalani (2010)

	Solid density (kg/m^3)	Fluid density (kg/m^3)	Bed height (m)	Orifice opening (mm)	Average particle size (mm)
Experiment	2650	1000	0.3	0.33	1
DEM-LBM	2700	1000	0.3	3	4.5

Initially, the system is set up with solids at a volume fraction of 0.55, which is lower than the desired packing prescribed in the experiment ($\alpha^s = 0.63$) to allow for interparticle forces to properly develop. Afterward, the solid particles are left to settle down to the prescribed volume fraction of 0.63 such that the total height of the silica sand submerged underwater is 0.3 m. The maximum packing limit, α_{max}, is set to 0.68 such that no numerical instabilities rise from the computation of the permanent contact pressure term. Settling is left long enough (approximately 18 seconds of simulation time) to ensure that the system is initially static and no particle or fluid movement is happening. After the particles had settled such that the sand bed is initially at rest, water is injected through the slot at controlled flowrates. For the first simulation case used to reproduce the results reported by Alsaydalani (2010), the in injection flow rates are 135.6, 235.5, 338.8, and 506 l/h. As for the second simulation case used to reproduce the DEM-LBM results reported by Cui et al. (2014), the injection flow rates are 0.25, 0.5, and 0.75 l/s, which are equivalent to 900, 1800, and 2700 l/h.

4 RESULTS AND DISCUSSION

The numerical results presented in this section focus on two aspects: (i) the development of excess pore water pressure in the vicinity of the water jet, and (ii) the deformation and mobilisation of sand particles in the sand bed. The latter involves the surface heave and the formation of cavities/fluidized zones around the location of injection. Both aspects should give insights on the model's performance regarding capturing micro and macro-scale interactions.

4.1 PORE WATER PRESSURE

The numerically calculated excess pore water pressure values along the centreline of the box are shown in comparison to both experimental and DEM-LBM numerical results in Figure 3 and Figure 4. From the simulation, we observe that the excess pore water pressure value peaks at the location of the injection slot. The excess pore water pressure is then dissipated gradually until it approaches a value of zero at the surface of the sand. For both validation cases, we find that approximately 60%-70% of the excess pore water pressure is dissipated in the lower 80 mm of the sand bed. Such high rate of dissipation can be referred to the high energy needed at the injection entrance to mobilize a portion of the sand mass. Above the lower 80 mm of the sand bed, the excess pore water pressure appears to vary nearly linearly with depth, indicating a steady flow velocity. These observations align with those reported by Alsaydalani (2010) and Cui et al. (2014) in the sense that the inlet velocity is higher than the critical velocity, beyond which, fluidization will occur.

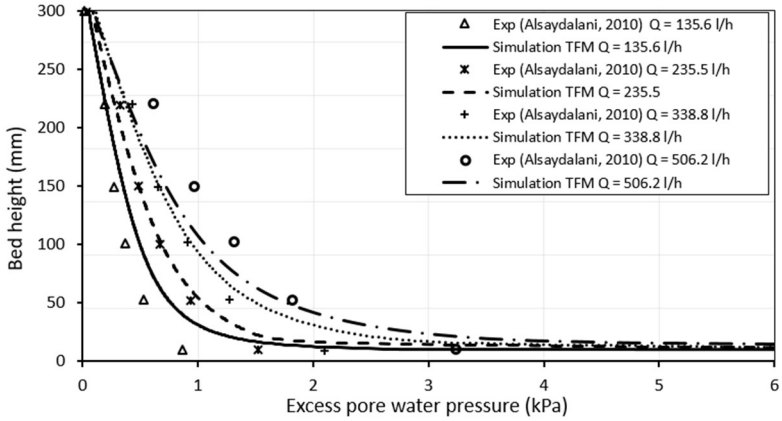

Figure 3. Excess pore water pressure along the centreline above the injection slot for different flowrates, TFM simulation vs. experimental results.

The results for excess pore water pressure obtained from the TFM simulations show good agreement with both experiment and DEM-LBM simulation in terms of the general trend and obtained values. The extent of mobilisation of solid particles, however, is difficult to investigate solely from the results of excess pore water pressure as it requires further investigation of the deformation of the sand bed.

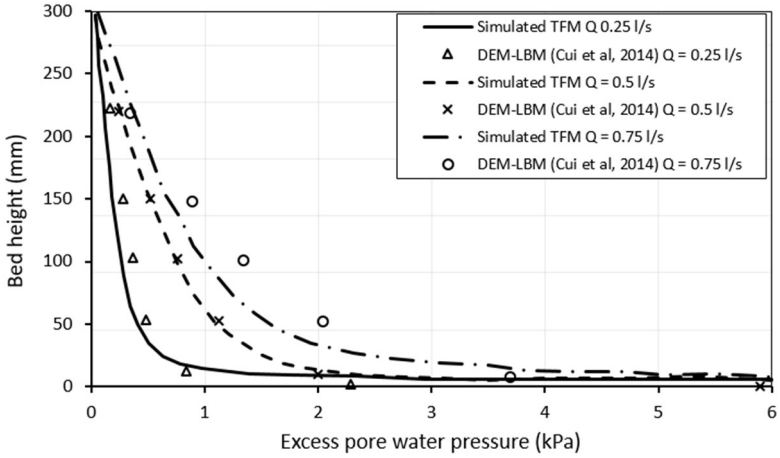

Figure 4. Excess pore water pressure along the centreline above the injection slot for different flowrates, TFM simulation vs. DEM-LBM results.

4.2 Surface heave and the extent of fluidization

To investigate the fluidized zones in our simulation, we look at the physical deformation of the sand bed from our simulation. As the sand surface or water above are not restrained (i.e., free surface condition), the upward driving force from injection is expected to cause heaving in the sand surface. This heave can be observed from the simulation (Figure 5(a)) and shows a decent agreement with the respective photographs from the experiment (Figure 5(b)). To visualise the fluidized zone around the injection slot, the colour scale representing solid volume fraction is shifted towards the far end of initial packing to display any possible mobilisation that could have happened (lower panel of Figure 5). The extent of the fluidized zone, although being slightly less than this from the experiment, shows a good representation of the fluidization area. Despite being mobilised, no cavities have been formed around the injection slot. This follow regime can be classified as a “static bed regime” as indicated by Cui et al. (2014), where no observable cavities are generated. This regime can be most closely interpreted as seepage flow, however, a fundamental difference from seepage is that the soil matrix does not remain intact and can be subjected to changes as injection conditions change.

A thorough investigation of the solid volume fraction for different flow rates is shown in Figure 6. It can be seen that particles are washed away in the vicinity of injection causing a reduction in the solid volume fraction of approximately 11%-15% and is directly proportional to the value of flow rate. Overall, the model showed good performance in capturing the characteristics of the onset of fluidization in comparison with the available experimental and numerical results. More importantly, the execution time for the two test cases considered in this study was nearly the same, which confirms the model’s scalability. This can provide a

reasonable preliminary assessment for the state of stresses and deformation in the vicinity of leakage and beyond. Nonetheless, the model suffers from some inherent drawbacks that should be taken into consideration.

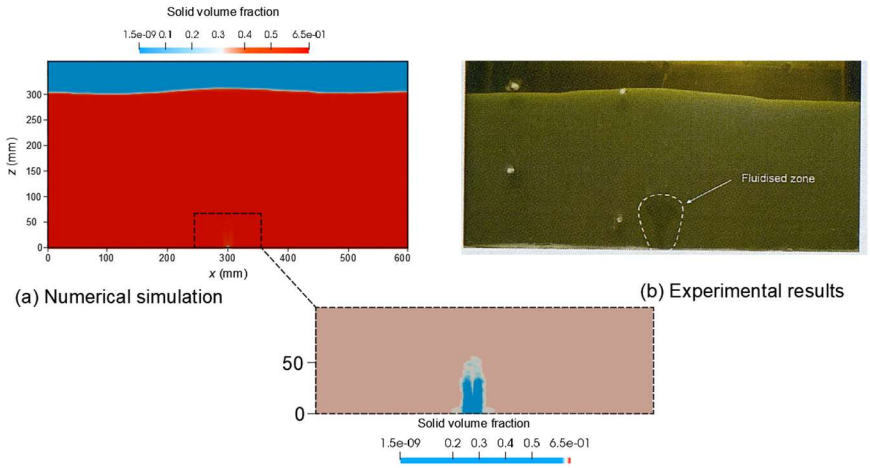

Figure 5. A comparison between the shape and the extent of the fluidized zone and surface heave, (a) TFM simulation vs. (b) experimental results from Alsaydalani (2010).

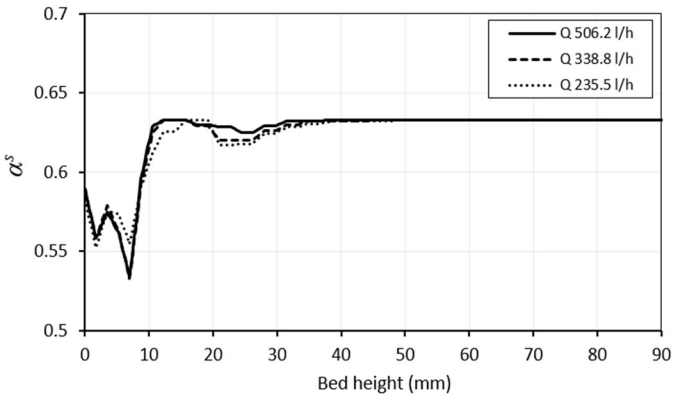

Figure 6. Variation of the solid volume fraction along the centreline for different flow rates.

4.3 Model limitations

The constant particle size used in the TFM simulation may not be a good representation of the actual soil. This issue was not observed in the comparison included here mainly because of the uniform nature of sands used in the experiment and numerical simulation. However, when dealing with actual soils, a much wider range of particle size distribution is most likely to be the case. Since the model deals with cell-averaged values of porosity, pressure and shear stresses, the actual coupling behaviour will be more difficult to capture. This issue becomes more critical in gap-graded soils where smaller particles are expected to be washed away into the pores of larger particles.

4.4 Conclusions

In this study, we tested the potential of the two-fluid model to simulate the internal fluidization in a submerged sand bed subjected to controlled injection (leakage) flow rates. The following observations and conclusions could be identified:

1 Our simulation results showed good agreement with reported experimental and numerical results of excess pore water pressure, surface heave and fluidized zone.

2 The model could decently capture the microscale-related interactions such as local fluidization as well as macro-scale behaviour such as surface heave.

3 Some inherent drawbacks to the model are identified such as its inability to account for particle size distribution, cohesion and particle shape.

4 The mesh-based adopted simulations' accuracy might be questionable when dealing with applications that involve fragmentation or highly convective flows in general.

5 Overall, the model can be a viable tool for preliminary assessment of coupled water-soil applications.

5 REFERENCES

Ali, H., and J. H. Choi. 2019. "A Review of Underground Pipeline Leakage and Sinkhole Monitoring Methods Based on Wireless Sensor Networking." *Sustainability* 11 (15). doi: ARTN 4007 10.3390/su11154007.

Alsaydalani, M.O.A. 2010. "Internal fluidization of granular material. PhD thesis." PhD thesis, University of Southampton.

Anderson, T. B., and Roy Jackson. 1967. "A fluid mechanical description of fluidized bed. Equations of motion." *Industrial Engineering Industry Fundamentals* 6:527-539.

Chauchat, Julien, Zhen Cheng, Tim Nagel, Cyrille Bonamy, and Tian-Jian Hsu. 2017. "SedFoam-2.0: a 3-D two-phase flow numerical model for sediment transport." *Geoscientific Model Development* 10 (12):4367-4392. doi: 10.5194/gmd-10-4367-2017.

Cheng, Zhen, Tian-Jian Hsu, and Joseph Calantoni. 2017. "SedFoam: A multi-dimensional Eulerian two-phase model for sediment transport and its application to momentary bed failure." *Coastal Engineering* 119:32-50. doi: 10.1016/j.coastaleng.2016.08.007.

Cook, Benjamin K., David R. Noble, and John R. Williams. 2004. "A direct simulation method for particle-fluid systems." *Engineering Computations* 21 (2/3/4):151-168. doi: 10.1108/02644400410519721.

Cui, Xilin, Jun Li, Andrew Chan, and David Chapman. 2014. "Coupled DEM–LBM simulation of internal fluidization induced by a leaking pipe." *Powder Technology* 254:299-306. doi: 10.1016/j.powtec.2014.01.048.

Deen, N. G., M. Van Sint Annaland, M. A. Van der Hoef, and J. A. M. Kuipers. 2007. "Review of discrete particle modeling of fluidized beds." *Chemical Engineering Science* 62 (1-2):28-44. doi: 10.1016/j.ces.2006.08.014.

Ding, Jianmin, and Dimitri Gidaspow. 1990. "A Bubbling Fluidization Model Using Kinetic Theory of Granular Flow." *AIChE Journal* 36 (4):523-538.

Gidaspow, D. 1994. *Multiphase Flow and Fluidization: Continuum and Kinetic Theory Descriptions*: Boston: Academic.

Hirche, Daniel, Fabian Birkholz, and Olaf Hinrichsen. 2019. "A hybrid Eulerian-Eulerian-Lagrangian model for gas-solid simulations." *Chemical Engineering Journal* 377. doi: 10.1016/j.cej.2018.08.129.

Ibrahim, A., and M. A. Meguid. 2020. "Coupled Flow Modelling in Geotechnical and Ground Engineering: An Overview." *International Journal of Geosynthetics and Ground Engineering* 6 (3). doi: ARTN 39
10.1007/s40891-020-00223-0.

Jenkins, J. T., and S. B. Savage. 1983. "A theory for the rapid flow of identical, smooth, nearly elastic, spherical particles." *Journal of Fluid Mechanics* 130 (1). doi: 10.1017/s0022112083001044.

Johnson, P. C., and R. Jackson. 1987. "Frictional-Collisional Constitutive Relations for Granular Materials, with Application to Plane Shearing." *Journal of Fluid Mechanics* 176:67-93. doi: Doi 10.1017/S0022112087000570.

Karoui, T., S. Y. Jeong, Y. H. Jeong, and D. S. Kim. 2018. "Experimental Study of Ground Subsidence Mechanism Caused by Sewer Pipe Cracks." *Applied Sciences-Basel* 8 (5). doi: ARTN 679
10.3390/app8050679.

Kuipers, J. A. M., K. J. Van Duin, Van Beckum, and W. P. M. Van Swaaij. 1992. "A numerical model of gas-fluidized beds." *chemical Engineering Science* 47 (8):1913-1924.

Lun, C. K. K., S. B. Savage, D. J. Jeffrey, and N. Chepurniy. 1984. "Kinetic theories for granular flow: inelastic particles in Couette flow and slightly inelastic particles in a general flowfield." *Journal of Fluid Mechanics* 140:223-256. doi: 10.1017/s0022112084000586.

Montella, E. P., M. Toraldo, B. Chareyre, and L. Sibille. 2016. "Localized fluidization in granular materials: Theoretical and numerical study." *Physical Review E* 94 (5). doi: ARTN 052905
10.1103/PhysRevE.94.052905.

Ostermeier, Peter, Stefan DeYoung, Annelies Vandersickel, Stephan Gleis, and Hartmut Spliethoff. 2019. "Comprehensive investigation and comparison of TFM, DenseDPM and CFD-DEM for dense fluidized beds." *Chemical Engineering Science* 196:291-309. doi: 10.1016/j.ces.2018.11.007.

Revil-Baudard, T., and J. Chauchat. 2013. "A two-phase model for sheet flow regime based on dense granular flow rheology." *Journal of Geophysical Research-Oceans* 118 (2):619-634. doi: 10.1029/2012jc008306.

Suzuki, K., J. P. Bardet, M. Oda, K. Iwashita, Y. Tsuji, T. Tanaka, and T. Kawaguchi. 2007. "Simulation of upward seepage flow in a single column of spheres using discrete-element method with fluid-particle interaction." *Journal of Geotechnical and Geoenvironmental Engineering* 133 (1):104-109. doi: 10.1061/(Asce)1090-0241(2007)133:1(104).

Tsuji, Y, T Kawaguchi, and T Tanaka. 1993. "Discrete particle simulation of two-dimensional fluidized bed." *Powder Technology* 77:79-87.

Tsuji, Y., T. Tanaka, and T. Ishida. 1992. "Lagrangian Numerical-Simulation of Plug Flow of Cohesionless Particles in a Horizontal Pipe." *Powder Technology* 71 (3):239-250. doi: Doi 10.1016/0032-5910(92)88030-L.

van der Hoef, M. A., M. Ye, M. van Sint Annaland, A. T. Andrews, S. Sundaresan, and J. A. M. Kuipers. 2006. "Multiscale Modeling of Gas-Fluidized Beds." In *Computational Fluid Dynamics*, 65-149.

van Zyl, J. E., M. O. A. Alsaydalani, C. R. I. Clayton, T. Bird, and A. Dennis. 2013. "Soil fluidization outside leaks in water distribution pipes - preliminary observations." *Proceedings of the Institution of Civil Engineers-Water Management* 166 (10):546-555. doi: 10.1680/wama.11.00119.

Vardoulakis, I., M. Stavropoulou, and P. Papanastasiou. 1996. "Hydro-mechanical aspects of the sand production problem." *Transport in Porous Media* 22 (2):225-244. doi: Doi 10.1007/Bf01143517.

Zhu, H. P., Z. Y. Zhou, R. Y. Yang, and A. B. Yu. 2007. "Discrete particle simulation of particulate systems: Theoretical developments." *Chemical Engineering Science* 62 (13):3378-3396. doi: 10.1016/j.ces.2006.12.089.

Zou, Yuhua, Chen Chen, and Limin Zhang. 2020. "Simulating Progression of Internal Erosion in Gap-Graded Sandy Gravels Using Coupled CFD-DEM." *International Journal of Geomechanics* 20 (1). doi: 10.1061/(asce)gm.1943-5622.0001520.